Analyst

PAPER

View Article Online
View Journal

Cite this: DOI: 10.1039/c4an00215f

# DNA hybridization detection with 100 zM sensitivity using piezoelectric plate sensors with an improved noise-reduction algorithm†

Ceyhun E. Kirimli,‡[a] Wei-Heng Shih[b] and Wan Y. Shih*[c]

Received 29th January 2014
Accepted 16th March 2014

DOI: 10.1039/c4an00215f

www.rsc.org/analyst

We have examined real-time, *in situ* hybridization detection of target DNA (tDNA) in a buffer solution and in urine using 8 μm-thick lead magnesium niobate–lead titanate (PMN–PT) piezoelectric plate sensors (PEPSs) about 1.1–1.2 mm long and 0.45 mm wide with improved 3-mercaptopropyltrimethoxysilane (MPS) insulation and a new multiple-parabola (>50) resonance peak position fitting algorithm. With probe DNA (pDNA) immobilized on the PEPS surface and by monitoring the first width extension mode (WEM) resonance frequency shift we detected tDNA in real time at concentration as low as $1 \times 10^{-19}$ M in urine (100 zM) with a signal to noise ratio (SNR) of 13 without DNA isolation and amplification at room temperature in 30 min. The present multiple-parabola fitting algorithm increased the detection of SNR by about 10 times compared to those obtained using the raw data and by about 5 times compared to those obtained using single parabola fitting. The detection was validated by *in situ* follow-up detection and subsequent visualization of fluorescent reporter microspheres (FRMs) coated with reporter DNA complementary to the tDNA but different from the probe pDNA.



## 1 Introduction

Cell-free DNA was first discovered by Mandel and Metais[1] in 1948 and became increasingly more important when mutant *ras* gene fragments were discovered in the blood of patients.[2,3] Since then, circulating DNA in the blood has been studied extensively for its diagnostic and prognostic association with various cancers such as bladder cancer,[4,5] breast cancer,[6–9] cervical cancer,[10,11] colorectal cancer,[12–16] hepatocellular carcinoma,[17–20] lung cancer,[21–25] lymphoma,[26–28] melanoma,[29–36] ovarian cancer,[37,38] pancreatic cancer,[39,40] and prostate cancer.[41–46] The passage of circulating DNA through the kidney barrier has been overlooked due to the selectivity of the nephron, and DNA fragments observed in urine have been mostly thought to have originated from organs and tissues of the urogenital tract. More recently, it has been found that low-molecular weight (LMW) DNA fragments from a distant organ could pass through kidneys.[47,48] The current standard method for detecting DNA is polymerase chain reaction (PCR). For transrenal DNA detection, PCR has limitations on the amplicon size[49] and potential inhibitions by co-isolated factors. Furthermore, the effectiveness of PCR could also be limited by DNA isolation techniques which are mostly utilized for isolating nuclear DNA from intact cells,[48] not particularly suitable for isolating short transrenal DNA fragments.[36,48,50] It would be desirable to have a real-time, label-free method that can detect transrenal DNA fragments in urine that does not depend on the DNA isolation techniques and is not limited by the lengths of the DNA fragments.

Current genetic detection technologies under development rely on fluorescence,[51–53] quartz crystal microbalance (QCM),[54,55] electrochemical,[56] binding of nano-metal particles,[57] surface plasmon resonance (SPR),[58] silicon-based microcantilever sensors as well as piezoelectric microcantilever sensors. For DNA detection, nanoparticle amplified QCM exhibited a concentration sensitivity of 1 pM.[59] Nanoparticle enhanced SPR exhibits a concentration sensitivity of 10–100 aM.[60] The electrochemical methods involving nanofibers and nanotubes also exhibited a concentration sensitivity of about 30 fM.[61] Nanowires[62–66] and nanotubes[67,68] exhibited concentration sensitivity ranging from 100 fM to 1 fM. Microcantilevers coupled to nano-metal particles exhibited 0.01 nM concentration sensitivity.[69] Although methods such as QCM, SPR, silicon-based microcantilever sensors as well as lead zirconate titanate (PZT) piezoelectric microcantilver sensors (PEMS)[70,71] were label-free, the sensitivity was still many orders of magnitude away from the attomolar ($10^{-18}$ M) requirement.[72] Similarly, the $10^{-16}$ M sensitivity achieved by magnetic bead isolation coupled with electrochemical

[a]*Lakehead University, Department of Chemistry, Thunder Bay, Canada. E-mail: ckirimli@lakeheadu.ca; Tel: +1-807-343-8450*

[b]*Drexel University, Department of Materials Science and Engineering, Philadelphia, Pennsylvania, USA. E-mail: shihwh@drexel.edu; Tel: +1-215-895-6636*

[c]*Drexel University, School of Biomedical Engineering, Science, and Health Systems, Philadelphia, Pennsylvania, USA. E-mail: shihwy@drexel.edu; Tel: +1-215-895-2325*

† Electronic supplementary information (ESI) available. See DOI: 10.1039/c4an00215f

‡ This work was carried out while a PhD student in the School of Biomedical Engineering, Science, and Health Systems at Drexel University in Philadelphia, PA 19104.

enhancement was not sufficient.[73] Nano-scale mechanical imaging by atomic force microscopy (AFM) can differentiate unhybridized single-stranded DNAs (ssDNAs) from hybridized double-stranded DNAs (dsDNAs) at attomolar sensitivity but it required a sophisticated instrument.[74] Although a GaN nanowire extended-gate field-effect-transistor could detect attomolar concentrations of the target DNA (tDNA) *in situ*[53] the detection signal (0.2 V) at $10^{-18}$ M was not very different from that (0.3 V) at $10^{-6}$ M making it unsuitable for DNA quantification. Streptavidin horseradish peroxidase functionalized carbon nanotubes could detect DNA at $10^{-18}$ M however it required labeling and was not *in situ*[75] while label-free carbon nanotube impedance biosensors could only detect DNA at 100 aM, not sufficient for clinical applications.[76] Electrochemical biosensors have been shown to reach attomolar sensitivity. However, they required electrocatalysis[77] or magnetic beads amplification[78] and were thus not label-free or real-time.

The lead magnesium niobate–lead titanate $(Pb(Mg_{1/3}Nb_{2/3})O_3)_{0.65}$–$(PbTiO_3)_{0.35}$ (PMN–PT) piezoelectric plate sensor (PEPS) is a new type of piezoelectric sensor consisting of solely a PMN–PT freestanding film 8 μm in thickness[79] thinly coated with a gold electrode on the two major surfaces and encapsulated with a thin 3-mercaptopropyltrimethoxysilane (MPS) electrical insulation layer (Fig. 1a). A receptor specific to a biomarker is immobilized on the surface of the electrical insulation layer. Binding of the target biomarker to the receptor on the PEPS surface shifts the PEPS length-extension-mode (LEM) (Fig. 1b) or width-extension mode (WEM) (Fig. 1c) resonance peak frequency, $f$. Detection of a target protein or target DNA (tDNA) marker is achieved by directly immersing a PEPS in the biological fluid and monitoring the LEM or WEM resonance frequency shift, $\Delta f$, in real-time. What is unique about PMN–PT PEPS is that the detection of $f$ is a result of binding stress induced polarization switching within the PMN–PT layer,[80] which was typically three orders of magnitude higher than that could be accounted for by the mass change alone.[81] As a result, PMN–PT PEPS has shown an unprecedented concentration sensitivity of 1.6 aM (960 copies per ml) in *in situ* tDNA detection without the need for amplification.[80] The reason we had different LEM and WEM modes was that we made PEPS longer than its width for ease of handling and ease of making. Ideally, one would explore WEM for detection because the higher frequency of WEM could offer better sensitivity. Although, in theory, one could use either the LEM or WEM peak for detection, in past practice, only the LEM peak was usable in liquid. The reason was that the width of the WEM peak was closely related to the transverse electromechanical coupling constant, $-k_{31}$.[81] The better the piezoelectric performance of the PMN–PT layer the wider the WEM peak. For a $-k_{31}$ of about 0.32 the $Q$ value – the ratio of the peak frequency to the width at half the peak height – would be about 10.[81] Such a wide WEM peak at around 3.5 MHz coupled with imperfect electrical insulation and insufficient signal processing made tracking any meaningful peak position shift difficult. Recently, Soylu *et al.* has found that coating MPS at pH = 9 and with a trace amount of water reduced the conductivity of the insulation layer by three orders of magnitude.[82] With such improvement, it may be possible to track the WEM peak position change with an improved peak position fitting algorithm. The advantage of using a WEM peak for detection is that the resonance frequency of a WEM peak is many times higher than that of the LEM peak. As a result, one may be able to further lower the detection concentration limit.

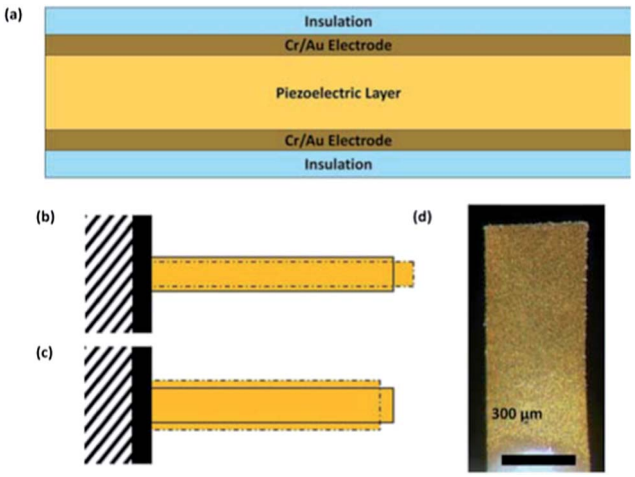


Fig. 1 A schematic of (a) the cross-section of a piezoelectric plate sensor (PEPS), (b) the first length extension mode (LEM), (c) width extension mode (WEM) vibration of a PEPS where the solid bars illustrate the initial position of the PEPS and the dashdotted shapes illustrate the extended positions, and (d) a top-view optical micrograph.

The goal of this study is to investigate how one can use a WEM peak of a PMN–PT PEPS with improved electrical insulation to detect short DNA fragments spiked in urine using a multiple-parabola peak position fitting approach. The hypothesis was that by fitting the WEM peak to more than one parabola with varying numbers of data points and by averaging the fitted peak positions one would be able to reduce the noise level for more meaningful tracking of the WEM peak frequency shift due to target DNA binding. We used 1762T/1764A Hepatitis B virus double mutation (HBV-DM) as the model tDNA as it was used in the previous study by an LEM peak with 1.6 aM sensitivity.[80] HBV-DM is a hepatitis B viral DNA variant comprised of adenine-1762 to thymine transversion and guanine-1764 to adenine transition which has been previously shown to be a risk factor for the development of hepatocellular carcinoma (HCC).[83,84] A high percentage (>60%) of HCC patients had HBV-DM in their sera.[85,86] We show that by fitting the WEM peak to an average of 50 parabolas we could increase the signal ($S$) to noise ($N$) ratio, SNR, by more than 10 times over the raw data and more than 5 times over single-parabola fitting and allowed meaningful tracking of the WEM peak frequency shift in real-time *in situ* detection of HBV-DM in urine with 100 zM (60 copies per ml) sensitivity without the need for DNA isolation or amplification.

## 2 Experimental

### 2.1 PEPS fabrication

Two PEPS (PEPS A and PEPS B) were used in this study. PEPS A was 1.2 mm long and 0.45 mm wide and PEPS B was 1.1 mm

 

long and 0.45 mm wide. The geometry of the sensor, about 1 mm long and 0.5 mm wide, was a compromise between ease of fabrication and sensitivity. Presently, the PEPS were fabricated manually. While making the PEPS smaller can increase the LEM and WEM frequencies and potentially further enhance the detection sensitivity it would be hard to accomplish manually. However, it should be noted that with presently available tools and automation, in the future, it is possible to make smaller PEPS. Briefly, PEPS A and PEPS B were fabricated from PMN–PT freestanding films 8 μm thick that were coated with 110 nm thick Cr/Au electrodes by thermal evaporation (Thermionics VE 90) and cut into 2.5 mm by 0.45 mm strips with a wire saw (Princeton Scientific Precision, Princeton, NJ). Gold wires 10 μm in diameter were glued to the top and bottom electrodes of each strip using a conductive glue (XCE3104XL, Emerson and Cuming Company, Billerica, MA). The rear end of the strip was fixed on a glass substrate with a nonconductive glue (Loctite 1C Hysol Epoxy Adhesive) to form the PEPS geometry. It was then poled at 15 kV $cm^{-1}$ at 90 °C for 60 min in an incubator (Digital Control Steel Door Incubator 10–180E, Quincy Lab). The dielectric constant of the PEPS was measured using an electrical impedance analyzer (Agilent 4294A) to be about 1800 with a loss factor of 2.5–3.7% at 1 kHz.

### 2.2 Electrical insulation

A PEPS was electrically insulated to stabilize the resonance peaks for in-liquid detection by a new 3-mercaptopropyltrimethoxysilane (MPS) (Sigma-Aldrich Co. LLC.) solution coating scheme involving improved MPS cross-linking at pH = 9.0 and with water.[82] First, the PEPS was cleaned in a Piranha solution (two parts of 98% sulfuric acid (Fisher) with one part of 30% hydrogen peroxide (Fisher)) for 1 min, followed by rinsing with water and ethanol. Before coating the PEPS with MPS at pH = 9.0, we dipped the PEPS in 50 ml of 0.01 mM MPS solution in ethanol (Fisher) with 0.5% of de-ionized (DI) water for 30 min to promote hydrolysis followed by rinsing with water and ethanol. It was then subject to 5 12 h of MPS coating in 50 ml of a 0.1% MPS solution with 0.5% of DI water in ethanol at pH = 9.0 (adjusted by adding KOH (Fisher)). For each 12 h of MPS coating, the PEPS was always rinsed with water and ethanol first before being immersed in a fresh 0.1% MPS solution at pH = 9.0 with 0.5% water. At the end of the 5th round of MPS coating, the PEPS was rinsed with DI water and ethanol before further coating with receptors for detection. After insulation, the resonance spectra of the PEPS were recorded using a portable AIM 4170C impedance analyzer (Array Solutions).

### 2.3 Resonance peak frequency determination

The phase-angle-*versus*-frequency resonance spectra of PEPS A and PEPS B in air (black) and in phosphate buffer saline (PBS) solution (red) are shown in Fig. 2a and b. Note that PEPS A had a $-k_{31} = 0.32$ and PEPS B had a $-k_{31} = 0.33$ and the WEM peaks of PEPS A and PEPS B were both at around 3.5 MHz with a $Q$ of around 10, reminiscent of the high $-k_{31}$ of both PEPSs. Also note that the baselines of the in-air and in-PBS spectra of the

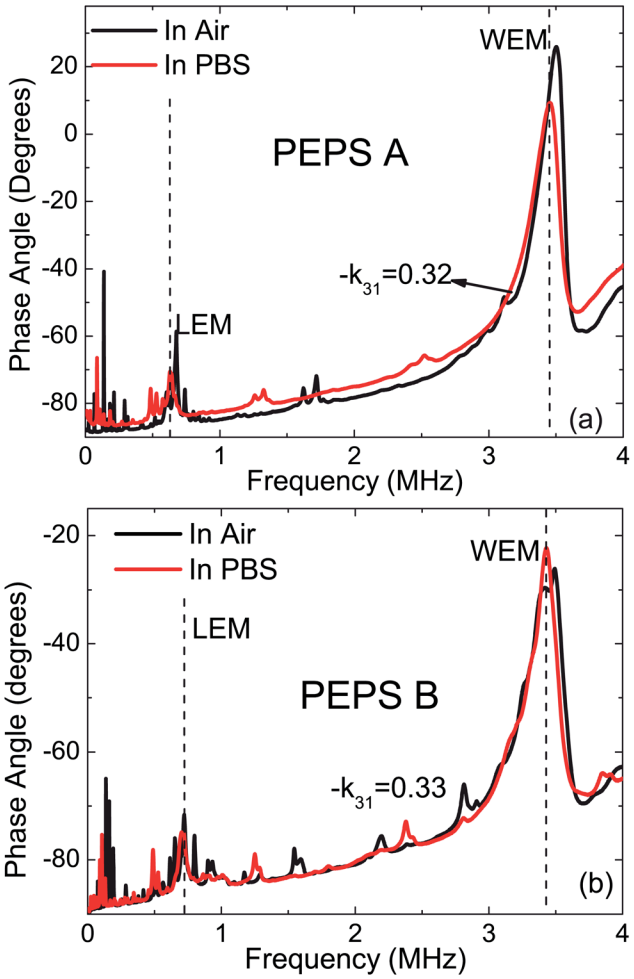


Fig. 2 In-air (black) and in-PBS (red) phase angle-*versus*-frequency resonance spectra of PEPS A (a) and PEPS B (b).

PEPSs were less than 1–2° apart, indicative of the effectiveness of the new insulation scheme.

For detection, phase angle-*versus*-frequency resonance spectra of a PEPS were recorded continuously using the AIM 4170C electrical impedance analyzer controlled by a laptop with a custom program written in MatLab. After each resonance-spectrum scan, the MatLab program recorded, analyzed the obtained spectrum, and determined the peak frequency as described below. A resonance peak frequency shift, $\Delta f$, *versus* time plot on the computer screen was refreshed after each resonance spectrum scan in real-time. The program also used the obtained peak frequency shift to adjust the start and stop frequencies for the next resonance-spectrum scan such that the next expected resonance frequency was roughly at the center of the frequency window. To determine the peak frequency, the raw resonance spectrum (black full squares in Fig. 3) was first smoothed by weighted-linear-least-square local regression as illustrated by the red curve in Fig. 3. The smoothed curve was then fitted to multiple (about 50) parabolas each with a different frequency range centered at the apparent peak frequency of the smoothed curve. As an example, one of the fitted parabolas is shown as the blue curve in Fig. 3 with its peak position denoted

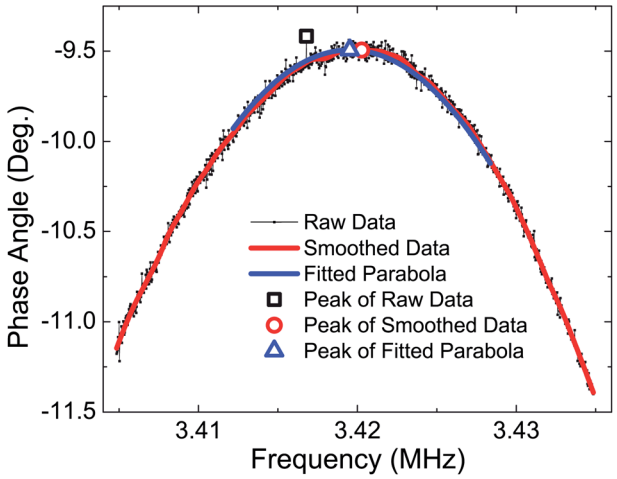


Fig. 3 Phase angle *versus* frequency resonance spectra where the raw data and the smoothed data are represented by the black full squares and the red curve, respectively, a parabola fitting using 540 data points is shown as the blue curve. The peak position of the raw data, that of the smoothed data and that of the fitted parabola are shown as the large black full square, red full circle and blue triangle, respectively.

by the blue triangle. Each parabola generated a fitted peak frequency. The final fitted peak frequency was the average of all the fitted parabola peak frequencies with outliers[87] excluded.

### 2.4 Target DNA, probe DNA, and reporter DNAs

The tDNA used was the same 200-nucleotide (nt) long single-stranded DNA (Integrated DNA Technologies) as used in the previous study[80] containing the nucleotide sequence of the Hepatitis B virus genome (GeneBank Accession #X04615) centered around the 1762T/1764A double mutation. Part of the sequence of the tDNA that contained the double mutation is shown in Table 1 where the two mutation sites were underlined. The probe DNA (pDNA) was a 16 nt long synthetic single-stranded DNA (Sigma) complementary to the 16 nt sequence of the tDNA centered at the double mutation site as shown in Table 1. The pDNA had a biotin with a 12-polyethyleneglycol (PEG) spacer at the 5′ end. The melting temperature of the pDNA to the tDNA was 47 °C as estimated under the experimental conditions[88] and listed in Table 1.

To immobilize the biotin-activated pDNA on the PEPS surface, the MPS-coated PEPS was first immersed in 200 μl of 5 mg ml$^{-1}$ maleimide activated biotin (Maleimide-PEG11-Biotin) (Pierce) in PBS for 30 minutes. The maleimide reacted with the thiol group on the MPS surface to immobilize the biotin on the PEPS surface. It was then followed by immersion of the PEPS in 200 μl of 1 μM streptavidin in PBS to bind streptavidin to the biotin on the PEPS surface. Afterwards, the PEPS was immersed in 200 μl of a 10 μM solution of the probe DNA in PBS for an

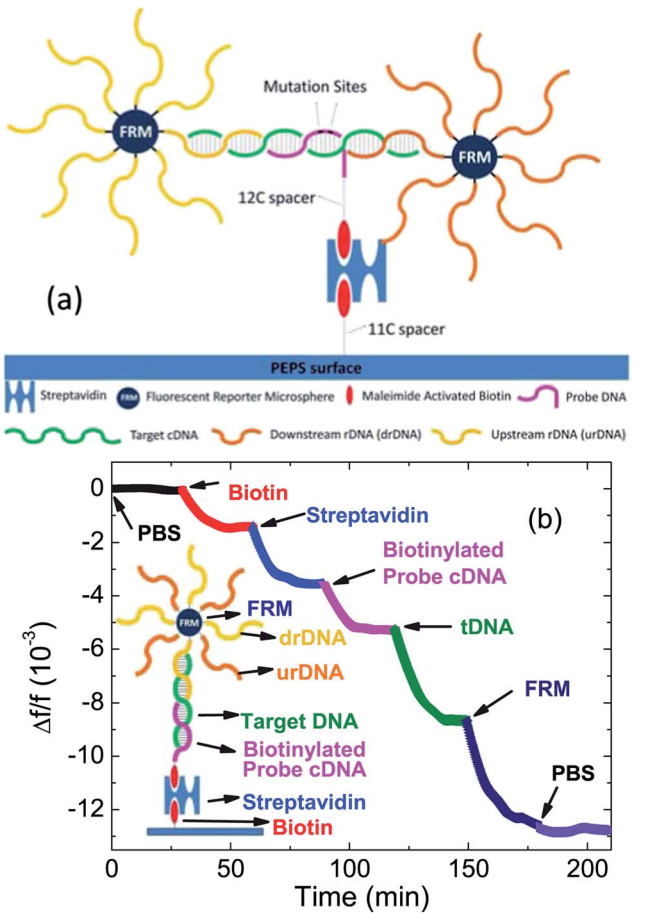


Fig. 4 (a) A schematic of the relations between tDNA, pDNA, urDNA and drDNA. pDNA is immobilized on the PEPS surface using a biotin–streptavidin–biotin sandwich. The 200 nts long tDNA (green) hybridizes to pDNA (pink) in the middle, and the upstream and downstream flanking regions hybridize with upstream (yellow) and downstream (orange) rDNA which are conjugated on FRMs (dark blue spheres) and (b) relative resonance frequency shift, $\Delta f/f$, of PEPS A during various steps of pDNA immobilization and tDNA detection. The inset in (b) shows a schematic of the molecules involved in the immobilization and detection steps.

Table 1 The sequences of tDNA, pDNA, upstream urDNA and downstream drDNA and the melting temperature, $T_m$, of the tDNA with pDNA, that of the tDNA with urDNA, and that of the tDNA with drDNA

| Type of DNA | Sequence (5′ to 3′) | $T_m$ (°C) |
|---|---|---|
| tDNA[a] | 5′…GGTTAATGATCTTTGT…3′ | — |
| pDNA | Biotin-5′-ACAAAGATCATTAACC-3′ | 47 |
| Upstream rDNA (urDNA) | Amine-5′ACAGACCAATTTATGCCTACAGCCTCCTAG-3′ | 76.3 |
| Downstream rDNA (drDNA) | Amine-5′-AATCTCCTCCCCCAACTCCTCCCAGTCTTT-3′ | 77.4 |

[a] Mutation sites are indicated by underlined bases.

 

hour to allow the biotin at the 5′ end of the pDNA to bind to the streptavidin on the PEPS surface. The details of the chemical reaction of the immobilization steps are shown in the ESI.†

There were two 30 nt long reporter DNAs (rDNAs) (Sigma). One was complementary to the sequence upstream of which was complementary to the pDNA and the other was complementary to the sequence downstream of which was complementary to the tDNA. The upstream rDNA was amine-activated with a 12-PEG spacer at the 5′ end while the downstream rDNA was amine-activated with a 7-PEG spacer at the 3′ end. The sequence of the upstream rDNA and that of the downstream rDNA are also shown in Table 1. Fig. 4a is a schematic that illustrates the relationships between the tDNA, the pDNA, the urDNA, and the drDNA. In real DNA fragments, mutation sites may be located anywhere in the fragments and in some cases the mutated sites may be too close to the edge for strong enough rDNA binding. Under such conditions, rDNAs in the opposite stream would permit binding of the rDNA to the captured tDNA on the sensor surface. For this reason, we included both upstream and downstream rDNAs in the study even though in the present synthetic tDNA the mutation sites were centrally located. The melting temperature for binding the upstream rDNA (urDNA) to the tDNA was 76.3 °C and that of the downstream rDNA (drDNA) to the tDNA was 77.4 °C, which are also listed in Table 1. Both drDNA and urDNA are immobilized on 6 μm size fluorescent reporter microspheres (FRM) as described previously[80,89] for *in situ* validation as well as for visualization of the detection.[80] In Fig. 4b, we plot the $\Delta f/f$ *versus* time of PEPS A during the various steps of pDNA immobilization followed by tDNA detection and the subsequent FRM detection. Steps of immobilization are illustrated in the inset in Fig. 4b.

### 2.5 Urine sample preparation

Urine samples were collected in 50 ml centrifuge tubes in a first morning sample collection fashion after emptying the bladder the previous evening. The samples were kept in a 4 °C refrigerator before detection. Blocking of non-specific binding is accomplished by dissolving 3% bovine serum albumin (BSA) in urine equilibrated to room temperature.

### 2.6 Flow setup

All the tDNA detections were carried out in a flow setup. A schematic of the flow system consisting of a polycarbonate detection chamber 18.5 mm long, 3.5 mm wide and 5.5 mm deep (volume = 356 μl), three reservoirs, and a peristaltic pump (Cole-Parmer 77120 – 62) interconnected with 0.8 mm wide tubing is shown in Fig. 5a. The PEPS was vertically placed in the center of the flow chamber with its major faces parallel to the flow as illustrated by the schematic shown in Fig. 5b. In each detection event, only one reservoir was connected to the detection chamber. The total volume of the liquid was 50 ml including the liquid in the reservoir, the detection chamber and the connecting tubing. In what follows, all detections were carried out with a flow rate of 1 ml $min^{-1}$ corresponding to an average flow velocity of 1.4 mm $s^{-1}$ at the PEPS surface. Furthermore, in this setup, the detection could transit from one

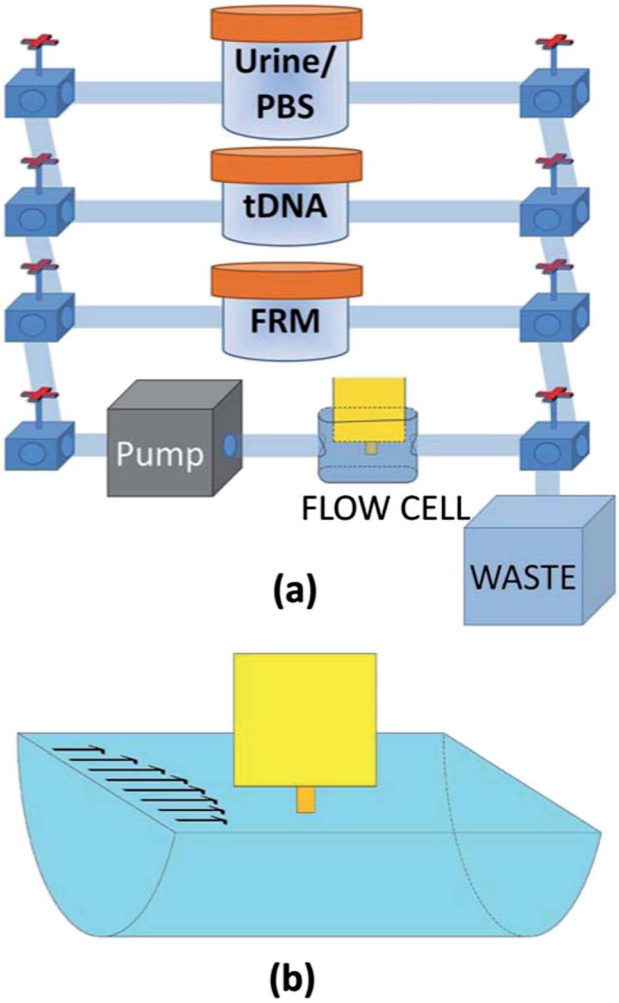


Fig. 5 (a) A schematic of the flow system and (b) a schematic of the flow cell where the PEPS is placed at the center of the laminar flow.

detection experiment involving the sample in one reservoir to another detection experiment involving the sample of another reservoir by turning the valves. Typically, a 20 second period for valves turning without data recording was sufficient for a smooth transition from one detection experiment to another.

## 3 Results

The theoretical first WEM and the first LEM resonance peak frequencies could be calculated[80] using $f = c/2w$ and $f = c/4L$, respectively, where $c = \sqrt{Y_{11}/\rho}$ was the sound velocity in the piezoelectric layer with $Y_{11} = 81$ GPa and $\rho = 7800$ kg $m^{-3}$ being the Young's modulus in the length and width directions and the density of the piezoelectric layer, respectively, and $w$ and $L$ are the width and the length of the PEPS, respectively. The theoretical first LEM and WEM peak frequencies were estimated to be 623 kHz and 3.44 MHz, respectively, for PEPS A and 718 kHz and 3.42 MHz, respectively, for PEPS B as indicated by the vertical dashed lines in Fig. 2(a) and (b).

tDNA detection was carried out using PEPS A in PBS with tDNA spiked at various concentrations to compare the signal-to-

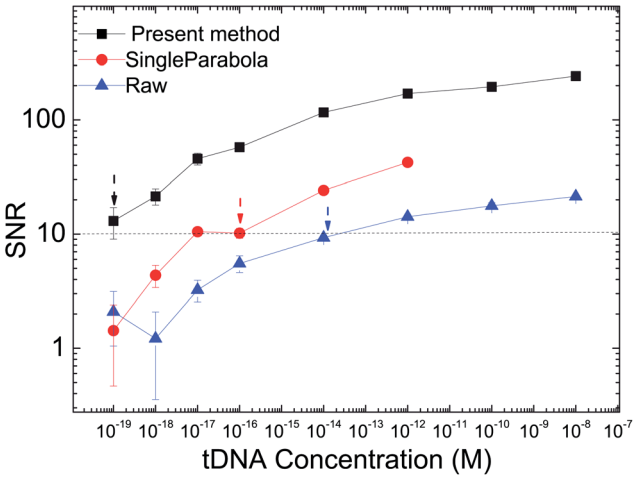


Fig. 6 Signal to noise ratio (SNR) *versus* tDNA concentration of tDNA detection in PBS by PEPS A where full squares, full circles, and full triangles denote SNRs obtained by the present multiple-parabola fitting algorithm, by single-parabola fitting (red circles), and by raw data, respectively. Arrows indicate the lowest concentrations with an SNR value of 10 for each method.

noise ratio (SNR) of the detection resonance frequency shift obtained by fitting the resonance peak frequency using the present multiple-parabola algorithm to those of the same detection but obtained using the raw data or using a single-parabola algorithm. The tDNA detection was immediately followed by FRM detection at a concentration of $10^5$ FRMs per ml as described previously.[80] The tDNA detection $\Delta f/f$ *versus* time of PEPS A and the corresponding $-\Delta f/f$ at $t = 30$ min *versus* tDNA concentration are included in the ESI.† In the present signal-to-noise (SNR) analysis, the signal was the average tDNA detection $\Delta f/f$ between $t = 25$ and 30 min and the noise was the standard deviation of $-\Delta f/f$ of the blank sample (*i.e.*, without tDNA). The resultant SNR *versus* tDNA concentration is shown in Fig. 6. Note all data points in Fig. 6 were the average of three independent runs for each concentration. As can be seen, the SNRs obtained by the present multiple-parabola fitting (full squares) were larger than 10 down to the tDNA concentration of $10^{-19}$ M. By convention, the lowest acceptable SNR is 3. The fact that the present detection with the multiple-parabola fitting algorithm exhibited an SNR of 10 at $10^{-19}$ M indicates high sensitivity of the PEPS detection. For comparison, we also plot the SNR obtained with the raw data (full triangles) and by single-parabola fitting (full circles). As can be seen, the present multiple-parabola fitting algorithm improved the SNR by about ten times from those obtained by the raw data and by about 5 times from those obtained by single-parabola fitting. Note the drop in SNR obtained from the raw data at $10^{-18}$ M was not meaningful, as the SNR at concentrations below $10^{-17}$ M were already below 3 – an indication that SNR values at below $10^{-17}$ M were not reliable. The positive tDNA detection with an SNR of 10 even at a tDNA concentration as low as 60 copies per ml was validated by the FRM detection immediately following the tDNA detection as described in the ESI.†

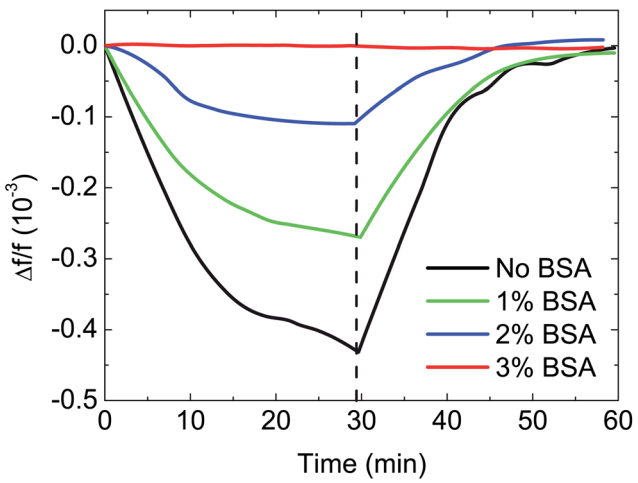


Fig. 7 Relative frequency shift, $\Delta f/f$, of PEPS B in urine at 1 ml $min^{-1}$ for 30 min followed by PBS washing at a flow rate of 6 ml $min^{-1}$ after the PEPS was initially blocked with 0, 1, 2 and 3 % BSA.

In the following, we applied the multiple-parabola fitting algorithm in the detection of DNA hybridization in urine using PEPS B. To determine the appropriate amount of BSA needed to block the PEPS surface from nonspecific binding, PEPS was first treated with a BSA solution with concentration ranging 0–3% followed by inserting the PEPS in flowing urine at a 1 ml $min^{-1}$ flow rate for 30 min followed by flowing a phosphate buffer saline (PBS) solution at a 6 ml $min^{-1}$ flow rate for 30 min. The resultant $\Delta f/f$ *versus* time in urine and the subsequent PBS washing with various amounts of BSA blocking is shown in Fig. 7. As can be seen, without BSA blocking, $\Delta f/f$ decreased in urine and subsequently recovered after PBS washing, indicating that the $\Delta f/f$ in urine was due to nonspecific binding by urine which could be washed off by flowing PBS. The nonspecific binding decreased with an increasing concentration of BSA blocking and with 3% BSA blocking it appeared that nonspecific binding by urine no longer occurred, *i.e.*, there was no resonance frequency down-shifting in urine and no resonance frequency up-shifting in PBS. In what follows, all detections were carried out with 3% BSA blocking.

Fig. 8a shows the $\Delta f/f$ *versus* time of tDNA detection in urine at $t = 0$–30 min followed by FRM detection at $t = 30$–60 min for tDNA concentrations of 0, $5 \times 10^{-20}$, $10^{-19}$, $10^{-18}$, $10^{-17}$, $10^{-15}$, $10^{-14}$, $10^{-10}$, and $10^{-8}$ M (0, 30, 60, 600, 6, 000, $6 \times 10^5$, $6 \times 10^6$, $6 \times 10^{10}$, and $6 \times 10^{12}$ copies per ml). Note that all the data points shown in Fig. 8a were the averages of three independent detections at each tDNA concentration. As can be seen, $\Delta f/f$ decreased with time in a dose responsive fashion. In addition, $\Delta f/f$ further decreased during the subsequent FRM detection validating that the $\Delta f/f$ observed during the tDNA detection was indeed due to the binding of the tDNA to the pDNA on the PEPS surface. The $-\Delta f/f$ at $t = 30$ min after tDNA detection and the $-\Delta f/f$ after FRM detection at $t = 60$ min are plotted *versus* tDNA concentration in Fig. 8b. Clearly, the $-\Delta f/f$ of tDNA detection ranges from $0.19 \times 10^{-3}$ at $5 \times 10^{-20}$ M (30 copies per ml) to $> 3.3 \times 10^{-3}$ when saturated at $10^{-10}$ and $10^{-8}$ M. Fig. 8a and b clearly illustrate that PEPS exhibited a 10 decade dynamic range in DNA detection in urine. Furthermore, from Fig. 8b, one can

 

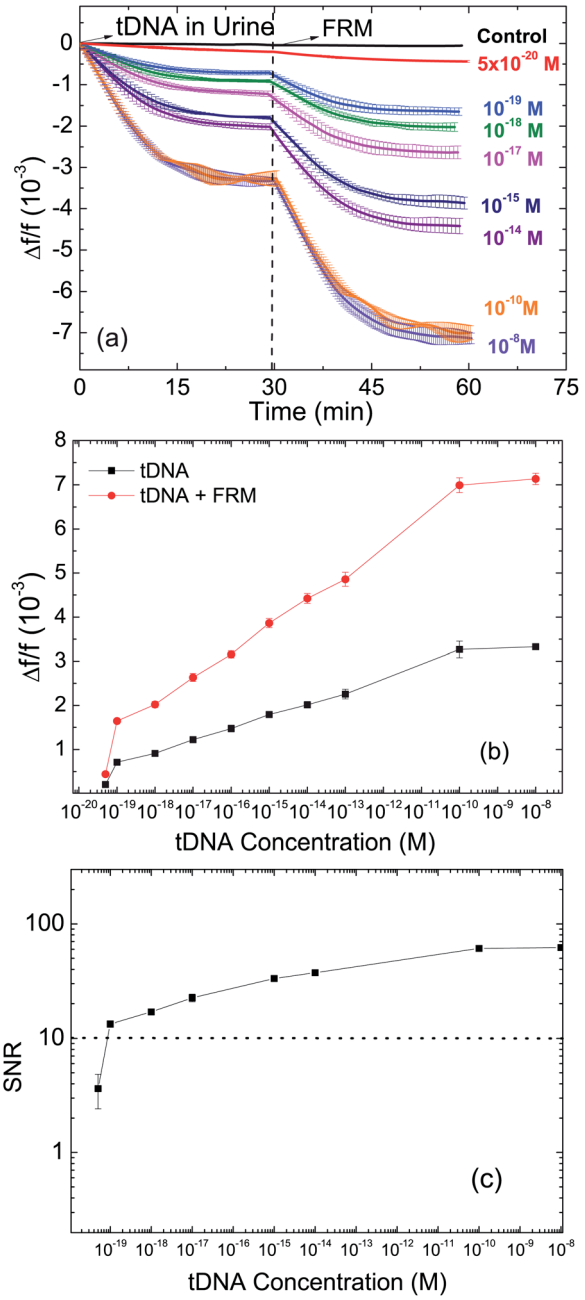


Fig. 8 (a) Relative resonance frequency shift $\Delta f/f$ *versus* time of tDNA detection at various concentrations in urine and (b) $-\Delta f/f$ at $t = 30$ min (tDNA hybridization) and at $t = 60$ min (tDNA hybridization plus FRM detection) *versus* tDNA concentration. (c) SNR *versus* concentration of tDNA graph plotted using data in (a).

see that $-\Delta f/f$ of the FRM detection following the tDNA detection was directly proportional to that of the tDNA detection alone, validating that the tDNA detection was indeed due to the binding of the tDNA to the pDNA on the PEPS surface. The SNR of the tDNA detection by PEPS B in urine was similarly analyzed where the signal denotes the average tDNA detection $\Delta f/f$ between $t = 25$ and 30 min and the noise denotes the standard deviation of $-\Delta f/f$ of the blank sample (*i.e.*, without tDNA). The resultant SNR *versus* tDNA concentration plot is shown in Fig. 8c. The SNR of the lowest concentration, $5 \times 10^{-20}$ M, was slightly above 3 with a standard deviation. For this reason the limit of detection for this study was chosen as $1 \times 10^{-19}$ M or approximately 60 copies per ml. Further, visual validation was carried out by examining the PEPS surface under a fluorescent microscope (Olympus BX51). Fluorescent micrographs of the FRMs captured on the PEPS surface following tDNA detection at various tDNA concentrations are shown in Fig. 9. As can be seen, the number of FRMs captured on the PEPS surface increased with an increasing tDNA concentration in a dose responsive fashion, further validating PEPS tDNA detection. The average number of FRMs on the PEPS surface *versus* tDNA concentration is also shown in Fig. 9g where each data point is the average of 6 images obtained at the same tDNA concentration.

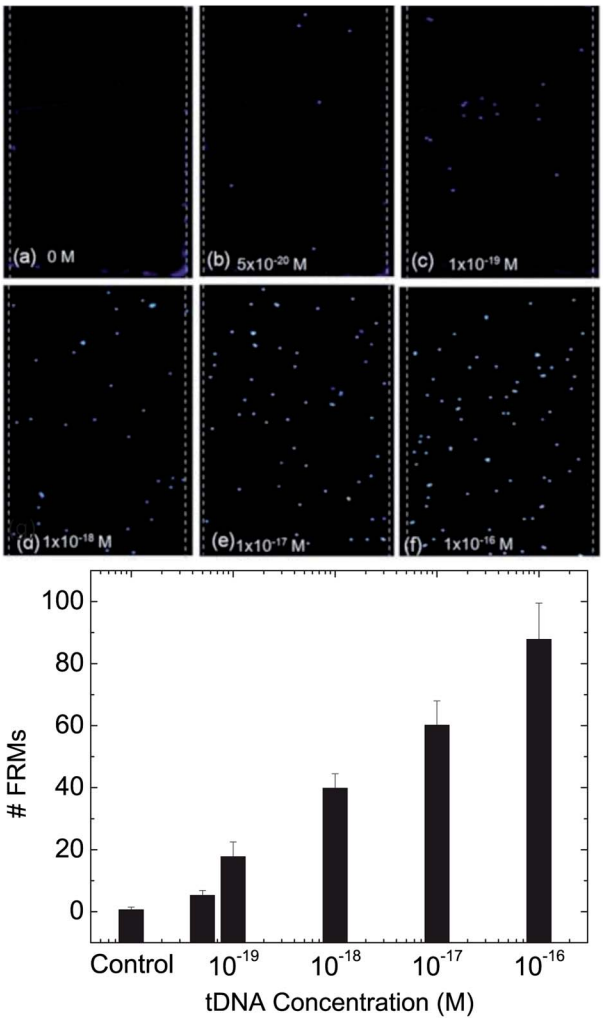


Fig. 9 Fluorescent micrographs of the PEPS surface after FRM detection followed by (a) 0 M, (b) $5 \times 10^{-20}$ M, (c) $1 \times 10^{-19}$ M, (d) $1 \times 10^{-18}$ M, (e) $1 \times 10^{-17}$ M and (f) $1 \times 10^{-16}$ M of tDNA detection. The width of PEPS B as denoted by the parallel dashed lines was 450 μm. Clearly, the number of FRMs captured on the PEPS surface increased with an increasing tDNA concentration in a dose responsive fashion validating the tDNA detection at a concentration as low as $5 \times 10^{-20}$ M. (g) Average number of FRMs captured on the PEPS surface *versus* tDNA concentration in urine.

# 4 Discussion

That a 60 copies per ml analytical sensitivity was achieved by both PEPS A in PBS and PEPS B in urine may be attributed to the similar $-k_{31}$ between PEPS A (0.32) and PEPS B (0.33). The sensitivity of a PEPS was related to its $-k_{31}$: the higher the $-k_{31}$ the more sensitive the PEPS.[81] With the results from both PEPS B and PEPS A it suffices to say that with improved MPS insulation and using the present multiple-parabola fitting algorithm a PEPS with $-k_{31} \geq 0.32$ exhibits an analytical sensitivity of better than 60 copies per ml, which is ≥16 times lower than that of the previous same tDNA detection in PBS using a PEPS with a similar $-k_{31}$ but with only single-parabola fitting.

# 5 Conclusions

We have examined real-time, *in situ* hybridization detection of tDNA in a buffer solution and in urine using 8 μm-thick PMN–PT PEPSs about 1.1–1.2 mm long and 0.45 mm wide with improved MPS insulation and a new multiple-parabola (>50) resonance peak position fitting algorithm. With pDNA immobilized on the PEPS surface and by monitoring the first width extension mode (WEM) resonance frequency shift we detected tDNA in real-time at concentration as low as $1 \times 10^{-19}$ M in urine (100 zM) with an SNR of >10 without DNA isolation and amplification at room temperature in 30 min. Note that there was no incubation time. 30 min was the time between when the sample was loaded and when the monitoring was stopped. The present multiple-parabola fitting algorithm increased the detection SNR by about 10 times from those obtained using the raw data and by about 5 times from those obtained using single parabola fitting. The detection was validated by *in situ* follow-up detection and subsequent visualization of FRMs coated with reporter DNA complementary to the tDNA but different from the pDNA.

# Acknowledgements

This work was supported in part by the Coulter-Drexel Translational Research Partnership grant and the Nanotechnology Institute of Benjamin Franklin Partnership of Southeastern Pennsylvania.

# References

1 P. Mandel and P. Metais, *C. R. Acad. Sci. (Paris)*, 1948, **142**, 241–243.
2 G. D. Sorenson, D. M. Pribish, F. H. Valone, V. A. Memoli, D. J. Bzik and S. L. Yao, *Cancer Epidemiol., Biomarkers Prev.*, 1994, **3**, 67–71.
3 V. Vasioukhin, P. Anker, P. Maurice, J. Lyautey, C. Lederrey and M. Stroun, *Br. J. Haematol.*, 1994, **86**, 774–779.
4 M. T. Valenzuela, R. Galisteo, A. Zuluaga, M. Villalobos, M. I. Nunez, F. J. Oliver and J. M. Ruiz de Almodovar, *Eur. Urol.*, 2002, **42**, 622–628; discussion 628–30.
5 M. Utting, W. Werner, R. Dahse, J. Schubert and K. Junker, *Clin. Cancer Res.*, 2002, **8**, 35–40.
6 H. Schwarzenbach, K. Pantel, B. Kemper, C. Beeger, F. Otterbach, R. Kimmig and S. Kasimir-Bauer, *Breast Cancer Res.*, 2009, **11**, R71.
7 J. M. Silva, J. Silva, A. Sanchez, J. M. Garcia, G. Dominguez, M. Provencio, L. Sanfrutos, E. Jareo, A. Colas, P. Espaa and F. Bonilla, *Clin. Cancer Res.*, 2002, **8**, 3761–3766.
8 B. Taback, A. E. Giuliano, N. M. Hansen, F. R. Singer, S. Shu and D. S. Hoon, *Cancer Res.*, 2003, **63**, 1884–1887.
9 N. Umetani, A. E. Giuliano, S. H. Hiramatsu, F. Amersi, T. Nakagawa, S. Martino and D. S. Hoon, *J. Clin. Oncol.*, 2006, **24**, 4270–4276.
10 A. Widschwendter, H. M. Muller, H. Fiegl, L. Ivarsson, A. Wiedemair, E. Muller-Holzner, G. Goebel, C. Marth and M. Widschwendter, *Clin. Cancer Res.*, 2004, **10**, 565–571.
11 W. Pornthanakasem, K. Shotelersuk, W. Termrungruanglert, N. Voravud, S. Niruthisard and A. Mutirangura, *BMC Cancer*, 2001, **1**, 2.
12 T. Lecomte, A. Berger, F. Zinzindohou, S. Micard, B. Landi, H. Blons, P. Beaune, P.-H. Cugnenc and P. Laurent-Puig, *Int. J. Cancer*, 2002, **100**, 542–548.
13 B. Lefebure, F. Charbonnier, F. Di Fiore, J. J. Tuech, F. Le Pessot, F. Michot, P. Michel and T. Frebourg, *Ann. Surg.*, 2010, **251**, 275–280.
14 B. M. Ryan, F. Lefort, R. McManus, J. Daly, P. W. Keeling, D. G. Weir and D. Kelleher, *Gut*, 2003, **52**, 101–108.
15 N. Umetani, J. Kim, S. Hiramatsu, H. A. Reber, O. J. Hines, A. J. Bilchik and D. S. Hoon, *Clin. Chem.*, 2006, **52**, 1062–1069.
16 T. deVos, R. Tetzner, F. Model, G. Weiss, M. Schuster, J. Distler, K. V. Steiger, R. Grtzmann, C. Pilarsky, J. K. Habermann, P. R. Fleshner, B. M. Oubre, R. Day, A. Z. Sledziewski and C. Lofton-Day, *Clin. Chem.*, 2009, **55**, 1337–1346.
17 K. Szymanska, O. A. Lesi, G. D. Kirk, O. Sam, P. Taniere, J. Y. Scoazec, M. Mendy, M. D. Friesen, H. Whittle, R. Montesano and P. Hainaut, *Int. J. Cancer*, 2004, **110**, 374–379.
18 G. D. Kirk, O. A. Lesi, M. Mendy, K. Szymanska, H. Whittle, J. J. Goedert, P. Hainaut and R. Montesano, *Oncogene*, 2005, **24**, 5858–5867.
19 K. C. A. Chan, P. B. S. Lai, T. S. K. Mok, H. L. Y. Chan, C. Ding, S. W. Yeung and Y. M. D. Lo, *Clin. Chem.*, 2008, **54**, 1528–1536.
20 I. H. Wong, Y. M. Lo, W. Yeo, W. Y. Lau and P. J. Johnson, *Clin. Cancer Res.*, 2000, **6**, 3516–3521.
21 S. Wang, T. An, J. Wang, J. Zhao, Z. Wang, M. Zhuo, H. Bai, L. Yang, Y. Zhang, X. Wang, J. Duan, Y. Wang, Q. Guo and M. Wu, *Clin. Cancer Res.*, 2010, **16**, 1324–1330.
22 A. Bearzatto, D. Conte, M. Frattini, N. Zaffaroni, F. Andriani, D. Balestra, L. Tavecchio, M. G. Daidone and G. Sozzi, *Clin. Cancer Res.*, 2002, **8**, 3782–3787.
23 Y. Liu, Q. An, L. Li, D. Zhang, J. Huang, X. Feng, S. Cheng and Y. Gao, *Carcinogenesis*, 2003, **24**, 1897–1901.
24 J. L. Ramirez, R. Rosell, M. Taron, M. Sanchez-Ronco, V. Alberola, R. de Las Penas, J. M. Sanchez, T. Moran, C. Camps, B. Massuti, J. J. Sanchez, F. Salazar and S. Catot, *J. Clin. Oncol.*, 2005, **23**, 9105–9112.

 

25 G. Sozzi, D. Conte, L. Mariani, S. Lo Vullo, L. Roz, C. Lombardo, M. A. Pierotti and L. Tavecchio, *Cancer Res.*, 2001, **61**, 4675–4678.
26 G. Hosny, N. Farahat and P. Hainaut, *Cancer Lett.*, 2009, **275**, 234–239.
27 W. Y. Au, A. Pang, C. Choy, C. S. Chim and Y. L. Kwong, *Blood*, 2004, **104**, 243–249.
28 I. Lei, L. Y. Chan, W. Y. Chan, P. J. Johnson and Y. M. Lo, *Clin. Cancer Res.*, 2002, **8**, 29–34.
29 R. E. Board, G. Ellison, M. C. Orr, K. R. Kemsley, G. McWalter, L. Y. Blockley, S. P. Dearden, C. Morris, M. Ranson, M. V. Cantarini, C. Dive and A. Hughes, *Br. J. Cancer*, 2009, **101**, 1724–1730.
30 A. Fujimoto, S. J. O'Day, B. Taback, D. Elashoff and D. S. Hoon, *Cancer Res.*, 2004, **64**, 4085–4088.
31 Y. Fujiwara, D. D. Chi, H. Wang, P. Keleman, D. L. Morton, R. Turner and D. S. Hoon, *Cancer Res.*, 1999, **59**, 1567–1571.
32 B. Taback, Y. Fujiwara, H. J. Wang, L. J. Foshag, D. L. Morton and D. S. Hoon, *Cancer Res.*, 2001, **61**, 5723–5726.
33 B. Taback, S. J. O'Day, P. D. Boasberg, S. Shu, P. Fournier, R. Elashoff, H. J. Wang and D. S. Hoon, *J. Natl. Cancer Inst.*, 2004, **96**, 152–156.
34 M. Shinozaki, S. J. O'Day, M. Kitago, F. Amersi, C. Kuo, J. Kim, H. J. Wang and D. S. Hoon, *Clin. Cancer Res.*, 2007, **13**, 2068–2074.
35 K. Koyanagi, T. Mori, S. J. O'Day, S. R. Martinez, H. J. Wang and D. S. Hoon, *Cancer Res.*, 2006, **66**, 6111–6117.
36 T. Mori, S. J. O'Day, N. Umetani, S. R. Martinez, M. Kitago, K. Koyanagi, C. Kuo, T. L. Takeshima, R. Milford, H. J. Wang, V. D. Vu, S. L. Nguyen and D. S. Hoon, *J. Clin. Oncol.*, 2005, **23**, 9351–9358.
37 H. M. Muller, S. Millinger, H. Fiegl, G. Goebel, L. Ivarsson, A. Widschwendter, E. Muller-Holzner, C. Marth and M. Widschwendter, *Clin. Chem.*, 2004, **50**, 2171–2173.
38 R. Zachariah, S. Schmid, N. Buerki, R. Radpour, W. Holzgreve and X. Zhong, *Obstet. Gynecol.*, 2008, **112**, 843–50.
39 T. Liggett, A. Melnikov, Q. L. Yi, C. Replogle, R. Brand, K. Kaul, M. Talamonti, R. A. Abrams and V. Levenson, *Cancer*, 2010, **116**, 1674–1680.
40 A. Castells, P. Puig, J. Mora, J. Boadas, L. Boix, E. Urgell, M. Sole, G. Capella, F. Lluis, L. Fernandez-Cruz, S. Navarro and A. Farre, *J. Clin. Oncol.*, 1999, **17**, 578–584.
41 P. J. Bastian, G. S. Palapattu, X. Lin, S. Yegnasubramanian, L. A. Mangold, B. Trock, M. A. Eisenberger, A. W. Partin and W. G. Nelson, *Clin. Cancer Res.*, 2005, **11**, 4037–4043.
42 M. Roupret, V. Hupertan, J. W. Catto, D. R. Yates, I. Rehman, L. M. Proctor, J. Phillips, M. Meuth, O. Cussenot and F. C. Hamdy, *Int. J. Cancer*, 2008, **122**, 952–956.
43 J. Ellinger, P. J. Bastian, K. I. Haan, L. C. Heukamp, R. Buettner, R. Fimmers, S. C. Mueller and A. von Ruecker, *Int. J. Cancer*, 2008, **122**, 138–143.
44 H. Schwarzenbach, C. Alix-Panabires, I. Mller, N. Letang, J.-P. Vendrell, X. Rebillard and K. Pantel, *Clin. Cancer Res.*, 2009, **15**, 1032–1038.
45 E. Sunami, M. Shinozaki, C. S. Higano, R. Wollman, T. B. Dorff, S. J. Tucker, S. R. Martinez, R. Mizuno, F. R. Singer and D. S. Hoon, *Clin. Chem.*, 2009, **55**, 559–567.
46 N. Mehra, M. Penning, J. Maas, N. van Daal, R. H. Giles and E. E. Voest, *Clin. Cancer Res.*, 2007, **13**, 421–426.
47 I. Botezatu, O. Serdyuk, G. Potapova, V. Shelepov, R. Alechina, Y. Molyaka, V. Ananev, I. Bazin, A. Garin, M. Narimanov, V. Knysh, H. Melkonyan, S. Umansky and A. Lichtenstein, *Clin. Chem.*, 2000, **46**, 1078–1084.
48 S. R. Umansky and L. D. Tomei, *Expert Rev. Mol. Diagn.*, 2006, **6**, 153–163.
49 Y. H. Su, M. Wang, T. M. Block, O. Landt, I. Botezatu, O. Serdyuk, A. Lichtenstein, H. Melkonyan, L. D. Tomei and S. Umansky, *Ann. N. Y. Acad. Sci.*, 2004, **1022**, 81–89.
50 A. Melnikov, D. Scholtens, A. Godwin and V. Levenson, *J. Mol. Diagn.*, 2009, **11**, 60–65.
51 D. M. Hammond, A. Manetto, J. Gierlich, V. A. Azov, P. M. Gramlich, G. A. Burley, M. Maul and T. Carell, *Angew. Chem., Int. Ed.*, 2007, **46**, 4184–4187.
52 F. Guo, M. I. Lapsley, A. A. Nawaz, Y. Zhao, S.-C. S. Lin, Y. Chen, S. Yang, X.-Z. Zhao and T. J. Huang, *Anal. Chem.*, 2012, **84**, 10745–10749.
53 Y. Chen and T. S. Seo, *Electrophoresis*, 2011, **32**, 1456–1464.
54 M. Passamano and M. Pighini, *Sens. Actuators, B*, 2006, **118**, 177–181.
55 K. Feng, J. Li, J. H. Jiang, G. L. Shen and R. Q. Yu, *Biosens. Bioelectron.*, 2007, **22**, 1651–1657.
56 R. Gasparac, B. J. Taft, M. A. Lapierre-Devlin, A. D. Lazareck, J. M. Xu and S. O. Kelley, *J. Am. Chem. Soc.*, 2004, **126**, 12270–12271.
57 S. J. Park, T. A. Taton and C. A. Mirkin, *Science*, 2002, **295**, 1503–1506.
58 L. He, M. D. Musick, S. R. Nicewarner, F. G. Salinas, S. J. Benkovic, M. J. Natan and C. D. Keating, *J. Am. Chem. Soc.*, 2000, **122**, 9071–9077.
59 X. Mao, L. Yang, X. L. Su and Y. Li, *Biosens. Bioelectron.*, 2006, **21**, 1178–1185.
60 L. K. Gifford, I. E. Sendroiu, R. M. Corn and A. Luptak, *J. Am. Chem. Soc.*, 2010, **132**, 9265–9267.
61 T. Yang, N. Zhou, Y. Zhang, W. Zhang, K. Jiao and G. Li, *Biosens. Bioelectron.*, 2009, **24**, 2165–2170.
62 G. Zheng, F. Patolsky, Y. Cui, W. U. Wang and C. M. Lieber, *Nat. Biotechnol.*, 2005, **23**, 1294–1301.
63 G. J. Zhang, Z. H. Luo, M. J. Huang, G. K. Tay and E. J. Lim, *Biosens. Bioelectron.*, 2010, **25**, 2447–2453.
64 A. Andreu, J. W. Merkert, L. A. Lecaros, B. L. Broglin, J. T. Brazell and M. El-Kouedi, *Sens. Actuators, B*, 2006, **114**, 1116–1120.
65 Z. Gao, A. Agarwal, A. D. Trigg, N. Singh, C. Fang, C. H. Tung, Y. Fan, K. D. Buddharaju and J. Kong, *Anal. Chem.*, 2007, **79**, 3291–3297.
66 J.-i. Hahm and C. M. Lieber, *Nano Lett.*, 2003, **4**, 51–54.
67 J. Wang, R. Polsky, A. Merkoci and K. L. Turner, *Langmuir*, 2003, **19**, 989–991.
68 H. Chang, Y. Yuan, N. Shi and Y. Guan, *Anal. Chem.*, 2007, **79**, 5111–5115.
69 M. Su, S. Li and V. P. Dravid, *Appl. Phys. Lett.*, 2003, **82**, 3562–3564.

70 K. Rijal and R. Mutharasan, *Anal. Chem.*, 2007, **79**, 7392–7400.
71 S. Zheng, J. H. Choi, S. M. Lee, K. S. Hwang, S. K. Kim and T. S. Kim, *Lab Chip*, 2011, **11**, 63–69.
72 F. Caruso, E. Rodda, D. N. Furlong, K. Niikura and Y. Okahata, *Anal. Chem.*, 1997, **69**, 2043–2049.
73 J. Wang, A. N. Kawde and M. Musameh, *Analyst*, 2003, **128**, 912–916.
74 S. Husale, H. H. Persson and O. Sahin, *Nature*, 2009, **462**, 1075–1078.
75 W. Gao, H. Dong, J. Lei, H. Ji and H. Ju, *Chem. Commun.*, 2011, **47**, 5220–5222.
76 T. Kurkina, A. Vlandas, A. Ahmad, K. Kern and K. Balasubramanian, *Angew. Chem., Int. Ed.*, 2011, **50**, 3710–3714.
77 L. Soleymani, Z. Fang, S. O. Kelley and E. H. Sargent, *Appl. Phys. Lett.*, 2009, **95**, 143701–143703.
78 O. A. Loaiza, S. Campuzano, M. Pedrero, M. I. Pividori, P. Garcia and J. M. Pingarron, *Anal. Chem.*, 2008, **80**, 8239–8245.
79 W. Y. Shih, H. Luo, H. Li, C. Martorano and W.-H. Shih, *Appl. Phys. Lett.*, 2006, **89**, 242913.
80 W. Wu, C. E. Kirimli, W. H. Shih and W. Y. Shih, *Biosens. Bioelectron.*, 2013, **43**, 391–399.
81 W. Wu, W. Y. Shih and W. H. Shih, *J. Appl. Phys.*, 2013, **114**, 064505.
82 M. C. Soylu, W.-H. Shih and W. Y. Shih, *Ind. Eng. Chem. Res.*, 2013, **52**, 2590–2597.
83 A. Munoz, J. G. Chen, P. A. Egner, M. L. Marshall, J. L. Johnson, M. F. Schneider, J. H. Lu, Y. R. Zhu, J. B. Wang, T. Y. Chen, T. W. Kensler and J. D. Groopman, *Carcinogenesis*, 2011, **32**, 860–865.
84 J. M. Yuan, A. Ambinder, Y. Fan, Y. T. Gao, M. C. Yu and J. D. Groopman, *Cancer Epidemiol., Biomarkers Prev.*, 2009, **18**, 590–594.
85 P. Arbuthnot and M. Kew, *Int. J. Exp. Pathol.*, 2001, **82**, 77–100.
86 S. Y. Kuang, P. E. Jackson, J. B. Wang, P. X. Lu, A. Munoz, G. S. Qian, T. W. Kensler and J. D. Groopman, *Proc. Natl. Acad. Sci. U. S. A.*, 2004, **101**, 3575–3580.
87 ASTM Standard E178-08, 2008, *Standard Practice for Dealing With Outlying Observations*, ASTM International, West Conshohocken, PA, 2008, DOI: 10.1520/e0178-08, http://www.astm.org/.
88 W. A. Kibbe, *Nucleic Acids Res.*, 2007, **35**, W43–W46.
89 C. E. Kirimli, W. H. Shih and W. Y. Shih, *Analyst*, 2013, **138**, 6117–6126.

 

## Supplemental Materials

### 1) Probe DNA immobilization

The maleimide of the maleimide-PEG-biotin linker reacted with the sulfhydryl of 3-mercaptopropyl-trimethoxysilane (MPS) on the MPS coating surface to form a thioester bond that covalently linked the maleimide-PEG-biotin on the MPS surface. The biotin of the immobilized maleimide-PEG-biotin then reacted with streptavidin to immobilize streptavidin on the PEPS surface. This was followed by the binding of biotin at the 5' end of the pDNA with the streptavidin bound on the biotin of the immobilized maleimide-PEG-biotin to finally immobilize pDNA on the PEPS surface. The steps of this immobilization are shown in Figure S1.

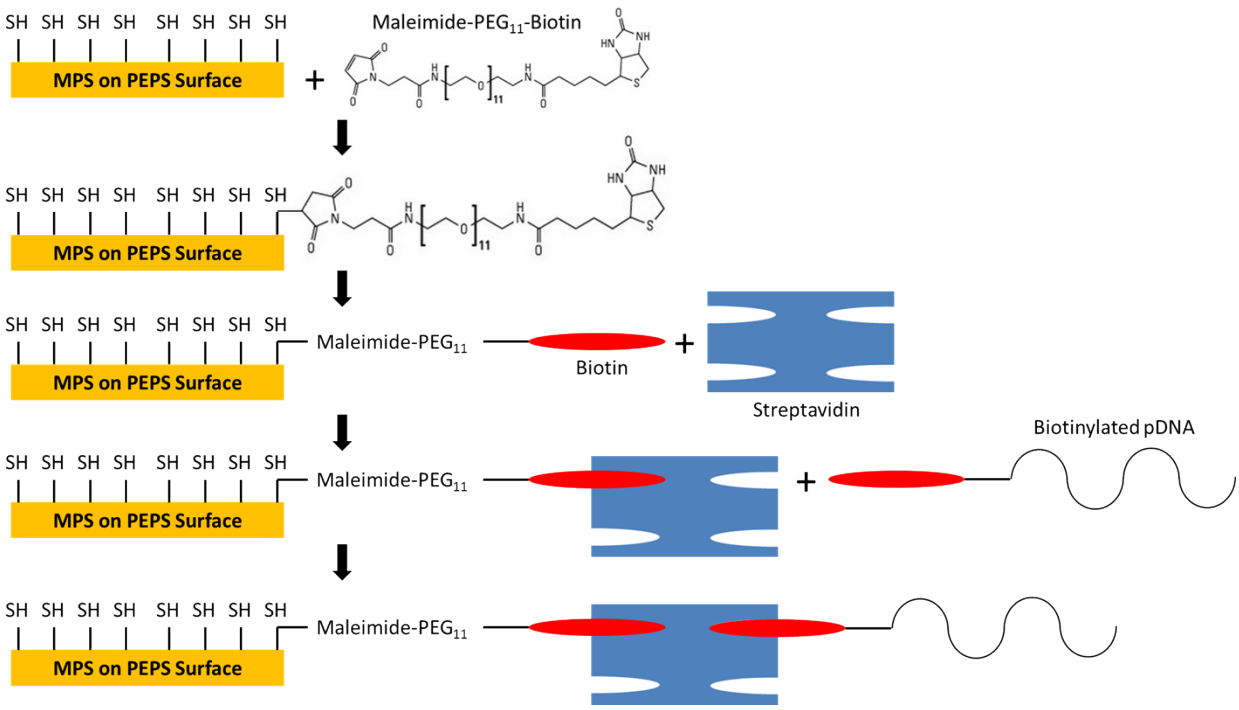


Figure S1. A schematic of the biotin-streptavidin-biotin sandwich immobilization scheme.

## 2) Detection of tDNA in PBS using PEPS A

Detections of different concentrations of tDNA in PBS using PEPS A are shown below. The resultant Δf/f versus time obtained using the multiple-parabola fitting algorithm as described in the manuscript is shown in Figure S2. Also shown is the Δf/f versus time of the following fluorescent microspheres FRM) detection also obtained by the multiple parabola fitting algorithm. Note all curves were the average of three independent detections at the same concentration. The pDNA immobilization and the tDNA preparation steps were carried out the same way as described in the text.

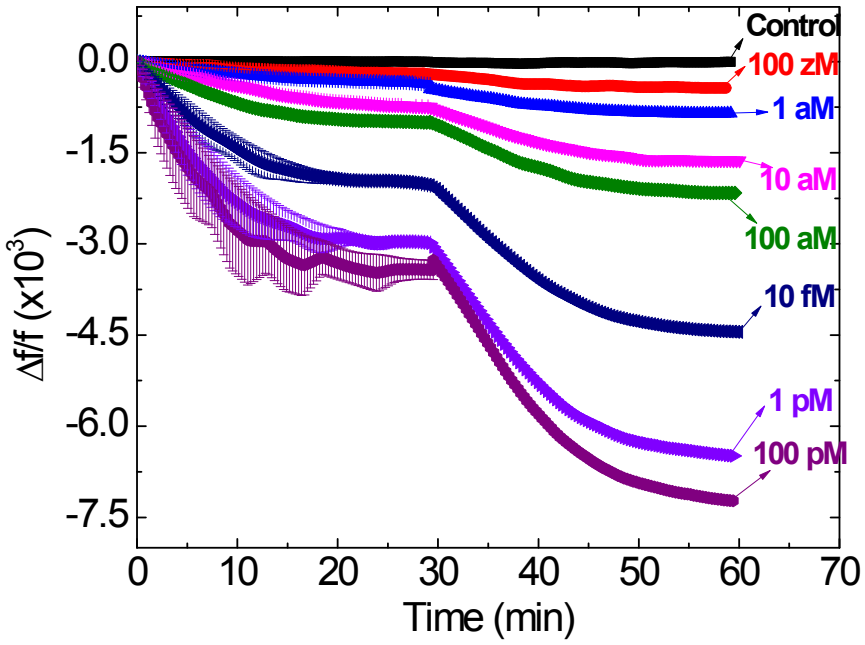


Figure S2. Δf/f versus time of tDNA detection and the following FRM detection at various tDNA concentrations in PBS as obtained using the multiple-parabola fitting algorithm.